Contact Resistance Change due to Air Gap Generation between Turns of NI REBCO Pancake Coils

Haru Sato and So Noguchi

***Abstract*—Rare-earth barium copper oxide (REBCO) magnets with excellent current characteristics under high temperature and high magnetic field has been developed for various applications worldwide. No-insulation (NI) REBCO coils allow currents to avoid flowing into normal-state transition regions due to turn-to-turn direct contacts, improving the thermal stability on the NI REBCO coils. The turn-to-turn contact resistances on NI REBCO coils are very important for thermal stability; but they change according to the turn-to-turn contact surface conditions. The contact condition is severely deteriorated when REBCO tape surfaces are not in contact.**

Our previous research pointed out that deformations on small-bore NI insert coils derived from strong stresses make some air gaps under high external magnetic field and high operating current, resulting in increase in the turn-to-turn contact resistances. In this paper, to investigate the air gap behaviors, an electromagnetic and stress simulation considering individual turn movements is conducted. A contact area ratio and a whole contact resistance of an NI REBCO pancake coil is computed. As the result, under the operating current of 50 A, the turn-to-turn contact conditions deteriorate by air gap generation between turns with the increase of the background fields. However, under 10 T, the turn-to-turn contact conditions improve as the operating current increases beyond 50 A. The air gap related with the distribution pattern of *BJR* stress, but not the strength of *BJR* stress.

***Index Terms*—no-insulation winding technique, REBCO magnet, stress simulation, turn-to-turn contact resistance.**

I. Introduction

SINCE ultrahigh magnetic fields are demanded for various applications such as MRI, NMR and so on [1]-[4], the development of high-temperature superconducting (HTS) magnets wound with rare-earth barium copper oxide (REBCO) coated conductors with excellent current characteristics under high temperature and high magnetic field attract attentions.

The increase in the thermal stability of REBCO magnets has been a major challenge in achieving the ultrahigh field generation for practical use. The appearance of a no-insulation (NI) winding technique proposed by Hahn [5] counters with the problem. An NI REBCO coil literally has no insulator between turns, allowing a current to avoid flowing into a normal-state transition region by directly carrying through contact surfaces between turns. The NI winding technique and its derivatives have been applied for many magnets: e.g. (1) the little big coil 3 (LBC3) generating 14.1 T in a background field of 31.1 T (the National High Magnetic Field Lab., USA) [6], (2) the toroidal field model coil (TFMC) of the SPARC project (the Massachusetts Institute of Technology and the commonwealth fusion systems, USA) [7], (3) the ultra-baby skeleton cyclotron (UBSC) magnet (Waseda University, Japan) [8], and so on. Commonly, these small-bore NI REBCO pancake coil has been placed in large-bore magnets to generate strong magnetic fields.

The turn-to-turn contact resistance is a key factor to improve the thermal stability of REBCO pancake coils [9]-[12]. It is strongly affected by the turn-to-turn contact surface condition in NI REBCO coils [13]-[15]. In particular, when REBCO tape surfaces are not in good contact, the contact condition is deteriorated: i.e., when there are gaps between turns, the contact resistances are extremely high like turn-insulated coils. As a matter of fact, the previous research [16] pointed out through simulations that when NI REBCO coils were subjected to strong stresses under high external magnetic field and large operating current, air gaps between turns were generated in some regions. Eventually, the turn-to-turn contact resistances of NI REBCO coils change due to air gaps according to external magnetic fields and operating currents. The air gaps in NI REBCO coils (i.e., increase in the turn-to-turn contact resistances) may downgrade the thermal stability. Nevertheless, the air gap behaviors have been not investigated so far.

In this research, in addition to an electromagnetic simulation on an NI REBCO pancake coil, a stress simulation considering the winding structure of the pancake coil are conducted. Based on the simulation, the turn-to-turn contact resistances of the whole coil and the air gaps between turns are investigated under different external magnetic fields and operating currents.

Manuscript received. This work was supported by the JSPS KAKENHI under Grant No. 20H02125. (*Corresponding author: So Noguchi.*)

H. Sato and S. Noguchi were with Graduate School of Information Science and Technology, Hokkaido University, Sapporo, 060-0814 Japan (e-mail: e-mail: mato@em.ist.hokudai.ac.jp, noguchi@ssi.ist.hokudai.ac.jp).

Color versions of one or more of the figures in this article are available online at http://ieeexplore.ieee.org

Digital Object Identifier will be inserted here upon acceptance.

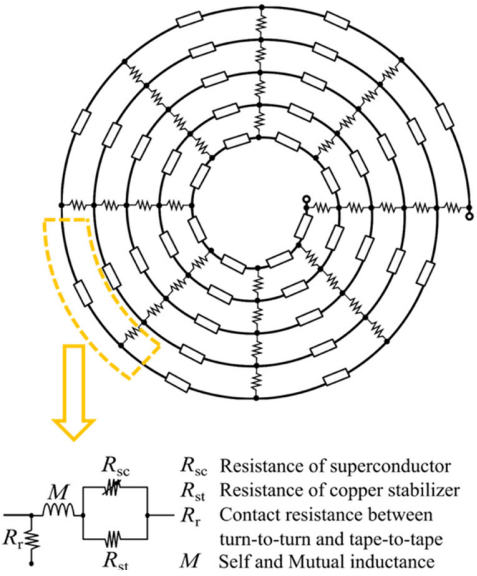

Fig. 1. Schematic view of the PEEC model.

II. Simulation Methods

An electromagnetic and stress simulation has been conducted to investigate the turn-to-turn contact conditions in this paper. Using a partial element equivalent circuit (PEEC) model (Fig. 1) as an electromagnetic simulation, local current distributions inside NI REBCO pancake coils are obtained [9]. Each partial element in PEEC is composed by the self-/mutual inductances M, the copper stabilizer resistance R_{st}, the REBCO resistance R_{sc} according to the *I-V* characteristic, and the turn-to-turn contact resistance R_{r}. The elements are connected in the radial and the circumferential directions in the PEEC model. The currents are obtained based on the Kirchhoff's law. The simulations were conducted under different operating currents and external magnetic fields. Note that the operating current is constant and stable on each simulation case.

A stress simulation is conducted with a finite element method (FEM). In order to represent the individual turn movement, the Karush-Kuhn-Tucker (KKT) condition [16] is applied onto turn-to-turn in the pancake coil model. Since the stress FEM simulation with the KKT condition is non-linear, the Newton-Raphson method is employed to solve it. Note that the friction between turns is not considered to simplify the model. Also, the innermost and outermost terminals of the NI REBCO pancake coil are assumed to be fixed. The governing equations for the stress simulation are

$$\frac{\partial \sigma_r}{\partial r} + \frac{1}{r}\frac{\partial \sigma_{r\theta}}{\partial \theta} + \frac{\sigma_r - \sigma_\theta}{r} + J_\theta B_z = 0 \qquad (1)$$

$$\frac{\partial \sigma_{r\theta}}{\partial r} + \frac{1}{r}\frac{\partial \sigma_\theta}{\partial \theta} + \frac{\sigma_{r\theta} + \sigma_{\theta r}}{r} - J_r B_z = 0 \qquad (2)$$

where σ_r, σ_θ, and $\sigma_{r\theta}$ are the radial, the azimuthal, and the shear stresses, respectively. J_r, J_θ, and B_z are the radial and the azimuthal current densities, and the axial magnetic field. They are obtained from the PEEC simulation.

From the results of the electromagnetic and stress simulations, the turn-to-turn contact ratio and resistance are investigated. The turn-to-turn contact resistance of the whole NI single pancake coil R_{pass} is obtained from the following equation [17]:

$$R_{\mathrm{pass}} = \sum_{i=1}^{N-1} \frac{\rho_i}{S_i} \qquad (3)$$

where ρ and N are the contact resistivity and the number of turns, respectively. Also, S_i is the actual turn-to-turn contact area of *i*th turn. When introducing the contact area ratio α_i on *i*th turn, obtained from the simulation results, $S_i = \alpha_i A_i$ where A_i is the ideal contact area of *i*th turn at the initial condition. In addition, the average contact area ratio β is defined as

$$\beta = \frac{\sum_{i=1}^{N-1} S_i}{\sum_{i=1}^{N-1} A_i}. \qquad (3)$$

considering contacts and separations between turns due to deformations of the coil.

TABLE I
Parameters of Simulation Models

Parameters	Values
REBCO Tape	
Width [mm]	4.0
Thickness [mm]	0.1
Copper matrix thickness [μm]	20.0
REBCO layer thickness [μm]	2.0
I_c @ 77 K, self-field [A]	120.0
Single Pancake Coil	
Coil i.d; o.d [mm]	60.0; 64.0
Number of turns	20
Turn-to-turn contact resistivity when in contact / not in contact [μΩ·cm²]	70.0 / Infinity
Coil height [mm]	4.0
Number of azimuthal divisions	19
Coil Inductance [μH]	50.3

TABLE II
Simulation Conditions

Parameters	Values
Operating temperature [K]	20.0
Operating Current [A]	0 to 400
External magnetic field [T]	5, 10, 20

III. Simulation Results

To investigate the average contact area ratio β and the contact resistance R_{pass}, we have simulated an NI REBCO single pancake coil. Tables I and II list the coil specifications and the simulation conditions, respectively.

A. Contact resistance and turn-to-turn contact

Figs. 2 and 3 show the contact resistance R_{pass} and the average contact area ratio β at the background fields of 5 T, 10 T, and 20 T. The area of turn-to-turn contacts decrease with the increase of the background fields. It also deteriorates as the operating current increase from 0 A to 50 A. That is, the turn-to-turn contact resistances increase. Meanwhile, under 10 T,

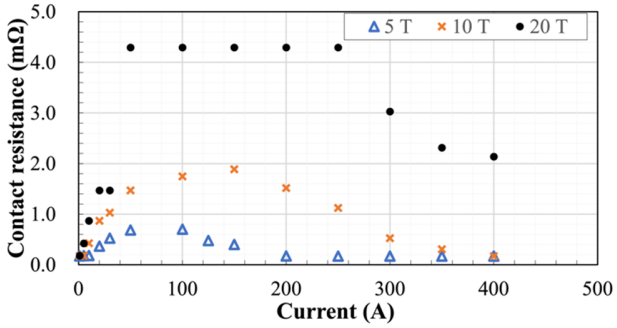

Fig. 2. Contact resistance R_{pass} at 5 T, 10 T and 20 T.

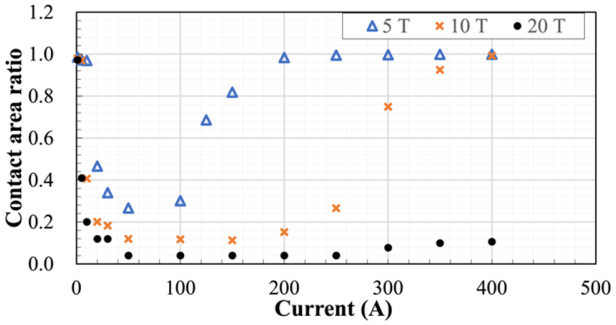

Fig. 3. Average contact area ratio β at 5 T, 10 T and 20 T.

the turn-to-turn contacts improve as the operating current increases beyond 50 A.

Fig. 4 shows the distribution of circumferential stresses at the operating current of 300 A with the background field of 20 T. As shown on the enlargement view in Fig. 4, the increase of the turn-to-turn contact resistance is caused by the air-gap appearance. The next section shows how the air-gaps appear.

B. Deformation of NI pancake coil

Fig. 4 show the distributions of radial displacement at the operating currents of 5 A (Case A), 50 A (Case B), and 300 A (Case C) in 5-T magnetic field and turn-to-turn contact area distribution in cases B and C. Air gaps between turns can be observed on the left half of the coil, where the circumferential stress is high. In Fig. 4, the red curve outside the coil shows the air-gap appearance region; while the blue curve shows the no-air-gap region around the current terminals. Consequently, the wide area of the coil has the air gaps between turns (~92%). Only ~8% has the good turn-to-turn contact condition.

The radial displacement is large with the increase of the operating current. In addition, with the operating current, the azimuthal displacement direction changes on Cases A, B, and C. The winding moves in the clockwise direction for Case B and in the anticlockwise direction for Case C. Fig. 5 indicates the radial displacement with different range from Fig. 4(a), which gives a more holistic view of the behaviors of the clockwise/counterclockwise displacements. In Case B, the radial displacement of outer turns is larger than that of inner turns; i.e., the radial displacement increases with the radius. It generates air gaps between turns. Eventually, from 0 A to 50 A,

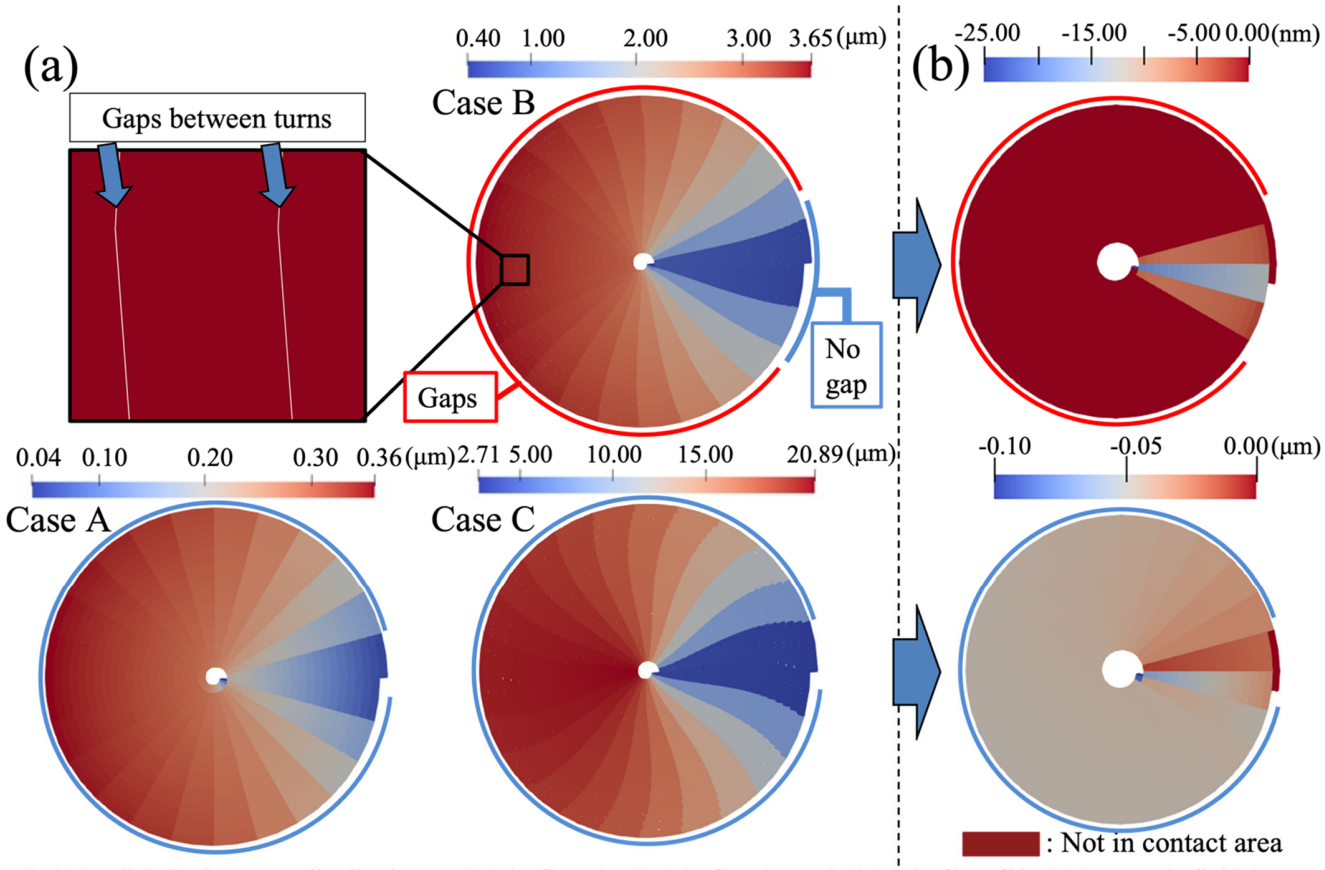

Fig. 4. (a) Radial displacement distributions at 5 A in Case A, 50 A in Case B, and 300 A in Case C in 5-T magnetic field (not to scale) and (b) turn-to-turn contact area distribution in Cases B and C.

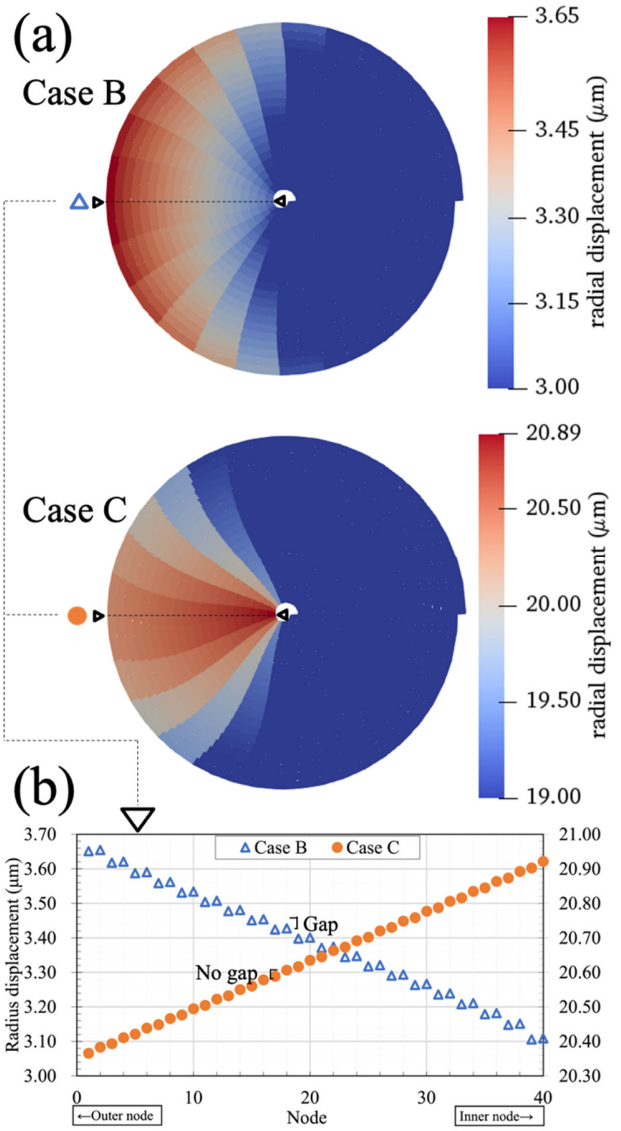

Fig. 5. (a) Radial displacements of Cases B and C with different range from Fig. 4 and (b) radial displacements on the opposite side of the end.

the turn-to-turn contact condition worsens resulting in the increase of the contact resistance. In Case C, the opposite tendency on the radial displacement is seen. The inner turns have larger radial displacement than the outer turns. Hence, the turn-to-turn contact condition is back to better with the increase of the operating current.

In Case A, since the radial displacements are small, small gaps appear in the whole coil. The contact resistance is sufficient small. Note that the average contact area ratio sharply decreases from 10 to 20 A, as shown on Fig. 3. In these conditions, the air-gap area would widen.

As seen on Case A in Fig. 4(a), a small radial displacement occurs between both two terminals, therefore, no air-gap is generated. Here, the blue curve outside the coils shows the no-air-gap area where there is no air gap between turns by physically contacting REBCO tapes. That is, the small radial displacement area has no air-gap, i.e. a low contact resistance.

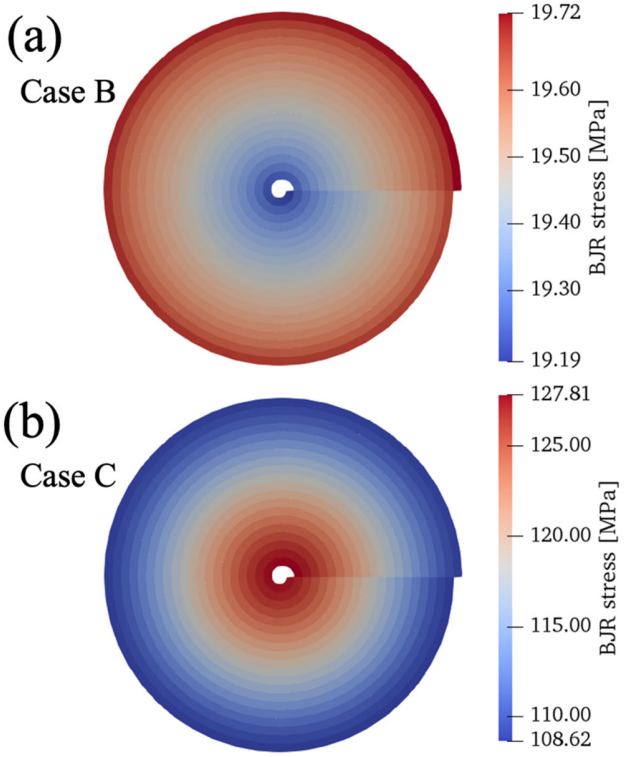

Fig. 6. *BJR* stress distributions of (a) Case B and (b) Case C.

From Figs. 4 and 5, it is possible to explain the contact resistance change as a function of the operating current.

C. BJR stress distribution

Fig. 6 shows the *BJR* stress distributions of Cases B and C. Note the strength range of stress are different between Cases B and C. In Case B, the *BJR* stress of outer turns is larger than those of inner turns; meanwhile, the *BJR* distribution of Case C is completely opposite. This result may be considered in conjunction with the results of the previous section. In Case B, the strong *BJR* stress on the outer turns results in the larger radial displacement than the inner turns. In Case C, the small *BJR* stress of outer turns prevents the air gap generation.

The air gap generation does not depend on the strength of the *BJR* stress. It is related with the distribution pattern of *BJR* stress.

V. Conclusion

From a stress simulation considering individual turn movement, the turn-to-turn contact conditions in a small-size insert NI REBCO pancake coil are investigated. As the result, the air gaps are generated depending on the operating current and the magnetic field. It affects the contact resistance.

Under a high external field, the turn-to-turn contact condition deteriorates at the low operating current, and it improves as the operating current increase. This phenomenon depends on the *BJR* stress distribution, not on the strength of *BJR* stress.

The change of the contact resistance would affect the thermal stability of NI REBCO pancake coils. It is necessary to investigate the thermal stability in the near future.

REFERENCES

[1] Y. Iwasa et al., "A High-Resolution 1.3-GHz/54-mm LTS/HTS NMR Magnet," *IEEE Trans. Appl. Supercond.*, vol. 25, no. 3, June 2015, Art no. 4301205.

[2] S. Yokoyama et al., "Research and development to the high stable magnetic field ReBCO coil system fundamental technology for MRI," *IEEE Trans. Appl. Supercond.*, vol. 27, no. 4, Jun 2017, Art. no. 4400604.

[3] H. Ueda et al., "Conceptual design of next generation HTS cyclotron," *IEEE Trans. Appl. Supercond*., vol. 23, no. 3, Jun. 2013, Art. no. 4100205.

[4] M. Niu, J. Xia, and H. Yong, "Numerical Analysis of The Electromechanical Behavior of High-Field REBCO Coils in All-Superconducting Magnets," *Supercond. Sci. Technol.*, vol. 34, no. 11, 2021, Art. no. 115005.

[5] S. Hahn, D. K. Park, J. Bascunan and Y. Iwasa, "HTS Pancake Coils Without Turn-to-Turn Insulation," *IEEE Trans. Appl. Supercond*., vol. 21, no. 3, pp. 1592-1595, June 2011.

[6] S. Hahn et al., "45.5-Tesla Direct-Current Magnetic Field Generated with A High-Temperature Superconducting Magnet," *Nature*, vol. 570, pp. 496-499, 2019.

[7] Z. S. Hartwig et al., "The SPARC toroidal field model coil program," submitted.

[8] R. Kumagai et al., "Fabrication and Experiments on a 1/2-Scale Demonstration NI-REBCO Coil System of a Skeleton Cyclotron for Cancer Therapy" submitted.

[9] T. Wang et al., "Analyses of Transient Behaviors of No-Insulation REBCO Pancake Coils During Sudden Discharging and Overcurrent," *IEEE Trans. Appl. Supercond.*, vol. 25, no. 3, June 2015, Art no. 4603409.

[10] S. Noguchi, K. Monma, H. Igarashi and A. Ishiyama, "Investigation of Current Flow Between Turns of NI REBCO Pancake Coil by 2-D Finite-Element Method," *IEEE Trans. Appl. Supercond.*, vol. 26, no. 3, pp. 1-5, April 2016, Art no. 4901205.

[11] Y. Yoshihara et al., "Evaluation Criterion for Determining Turn-to-Turn Contact Electrical Resistance Satisfying High Thermal Stability and Shortening Charging Delay in NI-REBCO Coils for MRIs," *IEEE Trans. Appl. Supercond.*, vol. 31, no. 5, Aug 2021, Art no. 4602005.

[12] H. Ueda, K. Naito, R. Inoue and S. Kim, "Deformation Analysis of No-Insulation REBCO Coils Considering Turn-to-Turn Contact Configuration," *IEEE Trans. Appl. Supercond.*, vol. 32, no. 6, Sept 2022, Art no. 4604205.

[13] M. Kitamura, K. Tsuyoshi, U. Nemoto, A. Ishiyama and S. Noguchi, "Numerical Evaluation of Transient Thermal Stability of No-Insulation REBCO Pancake Coils With a Noncontact Area Between Turns," *IEEE Trans. Appl. Supercond.*, vol. 32, no. 6, Sept 2022, Art no. 4605205.

[14] T. Lécrevisse and Y. Iwasa, "A (RE)BCO Pancake Winding With Metal-as-Insulation," *IEEE Trans. Appl. Supercond.*, vol. 26, no. 3, April 2016, Art no. 4700405.

[15] S. Noguchi, R. Miyao, K. Monma, H. Igarashi and A. Ishiyama, "Numerical Investigation of Metal Insulation Technique on Turn-to-Turn Contact Resistance of REBCO Pancake Coils," *IEEE Trans. Appl. Supercond.*, vol. 27, no. 4, June 2017, Art no. 7700505.

[16] K. Kodaka and S. Noguchi, "Stress and Deformation Analysis of REBCO Pancake Coils With Individual Turn Movement," *IEEE Trans. Appl. Supercond.*, vol. 33, no. 5, Aug 2023, Art no. 4600305.

[17] X. Wang et al., "Turn-to-turn contact characteristics for an equivalent circuit model of no-insulation REBCO pancake coil," *Supercond. Sci. Technol.*, vol. 26, 2013, Art. no. 035012.